Eur. Phys. J. Appl. Phys. **42**, 247–250 (2008)
DOI: 10.1051/epjap:2008060

THE EUROPEAN PHYSICAL JOURNAL APPLIED PHYSICS

Influence of Fe/Cr on nitrogen doped carbon nanotube growth

C.P. Ewels[1,2,a], A. Gloter[2], T. Minea[3], B. Bouchet-Fabre[4], S. Point[1], and C. Colliex[2]

[1] IMN, UMR6502 CNRS-Université de Nantes, 2 rue de la Houssinière, BP 32229, 44322 Nantes, France
[2] LPS, UMR8502 CNRS-Université Paris Sud, bâtiment 510, 91405 Orsay, France
[3] LPGP, UMR 8578 CNRS-Université Paris Sud, bâtiment 210, 91405 Orsay, France
[4] LFP, CEA/DSM/DRECAM/SPAM - CNRS URA 2453, CEA-Saclay, 91191 Gif-sur-Yvette Cedex, France

Received: 4 January 2008 / Received in final form: 6 March 2008 / Accepted: 6 March 2008
Published online: 30 April 2008 –

Abstract. Using electron energy loss spectroscopy in a 100 kV VG scanning transmission electron microscope we study nitrogen doped carbon nanotubes grown via electron cyclotron resonance (ECR) microwave plasma techniques. The process is controlled by direct current (dc) biasing the grid separating the ECR source and the substrate. We show that plasma induced sputtering of the ECR source wall (stainless steel) can lead to significant iron and chromium contamination of growth samples. We identify various Fe, Cr, Ni nitride phases, and propose a growth model based on nitridation-induced metal segregation of steel based FeCrN alloys. Trace Cr doping of nanotube catalysts appears a promising route for introducing large nitrogen concentrations into both single and multi-walled nanotubes and may accelerate nanotube growth rates.

PACS. 81.10.Bk Growth from vapor – 81.07.De Nanotubes – 52.50.Sw Plasma heating by microwaves; ECR, LH, collisional heating

1 Introduction

Plasma based nanotube growth techniques typically take place within stainless steel growth chambers, yet little attention has been paid in the literature to the possibilities for environmental sample contamination. While such effects are likely to be negligible for macro- and mesoscopic plasma studies, once samples become nanoscopic, trace contamination can become important. In the current study we examine the growth of carbon nanotubes (CNTs) via electron cyclotron resonance microwave plasma enhanced chemical vapour deposition (ECR-PECVD). Environmental contamination is observed and the result is a rich and complex chemistry, with important implications for nitrogen doping of carbon nanotubes. The work highlights the necessity for chemical elemental analysis of all synthesis studies to avoid potential misinterpretation of results.

ECR-PECVD is a versatile technique for growing and analysing CNTs, since there are many parameters such as gas feedstock and pressure, growth time, and plasma voltage that can be precisely controlled [1–3]. In addition there is the possibility for many in situ spectroscopic techniques allowing compositional analysis of the plasma. Finally the combination of efficient ECR which gives high density plasmas and the control of the ion flux on the substrate by dc grid biasing means that tubes can be grown at relatively low temperatures and mainly perpendicular to the substrate [2], encouraging growth far from thermal equilibrium. Moreover, this plasma process can potentially produce structures not attainable through higher temperature growth techniques or chemical vapour deposition (CVD). Thus, although not yet a technique suitable for large scale production of nanotubes, ECR-PECVD is nonetheless appropriate for analytical studies such as those presented here.

2 Method

The carbon nanotubes we study have been grown using the original dual PVD/PECVD process, described elsewhere [1]. Both steps of the deposition process employ the distributed electron cyclotron resonance plasma (DECR). The deposition pressure is low (0.2 Pa) imposed by the ECR condition. Thus, high density plasma is created in the ECR source. The substrate-holder is grounded and can be heated up to 900 °C.

A Ni catalyst thin film, ∼4 nm thick, was deposited onto the substrates (500 nm thermal SiO_2 on Si wafer) following the first step (PVD) of the process [1]. The growth temperature was 700 °C, enough to reorganise the Ni film into nanoparticles. Nanotube growth then occurred using an ECR-PECVD plasma in a mixture of acetylene/ammonia (1:2) with a grid bias of +200 V. Previous

[a] e-mail: chris.ewels@cnrs-imn.fr

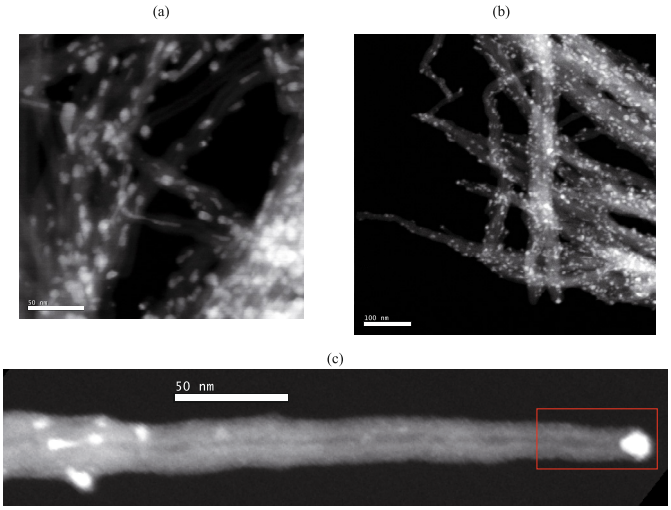

Fig. 1. HADF images of nanotube samples after (a) one hour (b) two hours of plasma growth. (c) Close-up of tube from sample (b) clearly showing the nanotube cavity, metal along the nanotube core and metal catalyst particle at the tube tip. Red box shows location used for spectral image maps in Figure 4.

plasma characterization has shown strong correlation between the grid potential and the plasma potential [4]. Growth time was either one or two hours; all other experimental parameters were kept fixed. The resultant deposit contains essentially multi-walled carbon nanotubes (MWNTs) [5].

The nanotubes were detached from the substrate by sonication for 15 min and then deposited on transmission electron microscopy (TEM) grids for electron energy loss spectroscopy (EELS) measurements, using a 100 kV scanning transmission electron microscope (VG BH501) equipped with a high angle annular dark field (HADF) detector. This permits mapping of electron energy loss with a spatial resolution of 0.7 nm and energy resolution of 0.7 eV before spectral deconvolution, 0.3 eV after deconvolution [6]. Chemical maps were obtained by acquisition of typically 64×64 spectra over an area of around 30×30 nm. At each pixel the EELS spectrum in the energy range from 200 to 900 eV is acquired and can then be further extracted for analysis. EELS acquisition time was chosen from 10 to 100 ms depending on the required signal to noise ratio. The following study uses core-loss EELS since this allows unambiguous identification of chemical species within the sample, as well as providing details of the chemical environment through the fine structure of the core-loss spectrum.

3 Results

Figure 1 shows typical HADF images for samples prepared over one hour (Fig. 1a), and two hours (Fig. 1b). In addition to carbon nanotubes, both samples show a high density of metal nanoparticles on the tube surfaces, as well as embedded in the amorphous regions, and also within the nanotube cores.

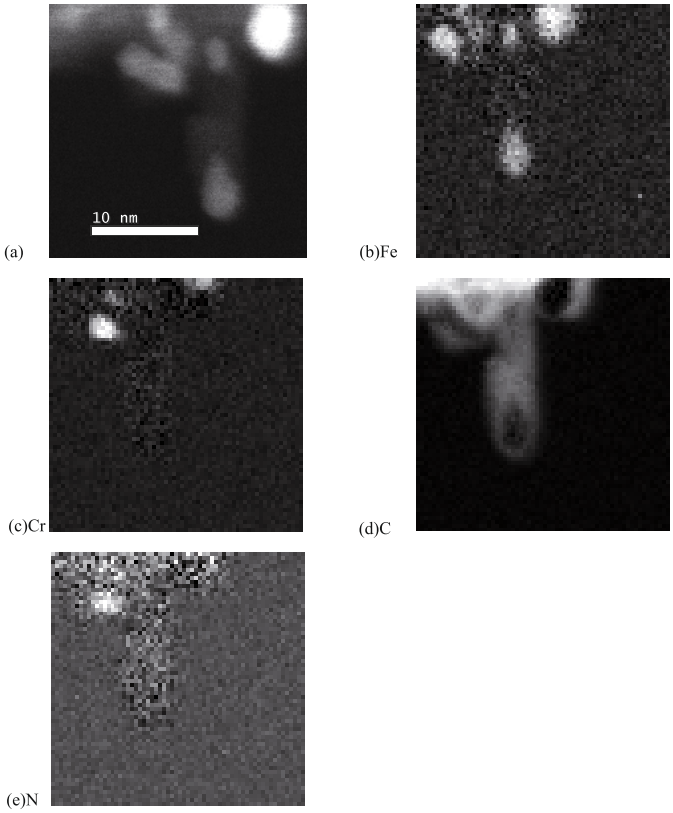

Fig. 2. Nanotube growth in the one-hour sample from a Fe particle. (a) HADF image, (b–f) core-EELS elemental maps showing distribution of (b) Fe (c) Cr (d) C π^* (e) N. Spectra taken in a grid of 64×64 pixels. Chemical maps are generated through integration of the K-edge (L2, 3) signal for C and N (Fe and Cr) after background subtraction. N and Cr are correlated (and anti-correlated with carbon). The segregation Fe/CrN_x is visible in the metal particles at the image top.

Elemental analysis of the EELS spectra show that both samples contain Fe and Cr, neither of which were deliberately added to the growth chamber. Ni metal typically contains trace Cr, however the commercial Ni source used here (Goodfellow®) is >99% pure, so this seems an unlikely source. Fe and Cr introduction must occur either before or during nanotube growth, since we observe Fe in the nanotube cores. The primary candidate is plasma etching/sputtering of the chamber. This unexpected phenomenon can be related to the grid biasing and is discussed further below. Stainless steel (Fe) contains high concentrations of Cr, as well as other alloying elements such as Ni, consistent with the metals we observe. Nonetheless the experimental conditions were still appropriate for growth of multiwalled carbon nanotubes.

In the one hour sample there are many nanoscale Fe and Cr particles. The Cr particles nearly always appear alongside a Fe particle (see Fig. 2). EELS elemental mapping shows high N content in the Cr particles, not the case for Fe. From the EELS spectra the Cr/N ratio in the CrN_x particles varies between $x = 0.9$ and 1.5 (despite our beam size being smaller than the typical Cr particle size, there will be some incorporation of signal from

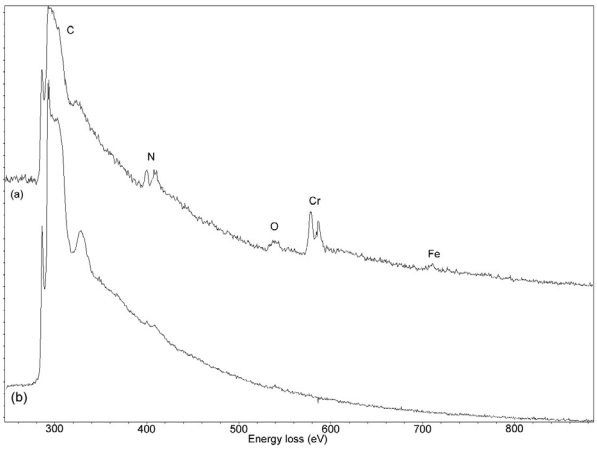

Fig. 3. EELS spectra of the two-hour growth sample for (a) a CrN_x and neighbouring Fe nanoparticle at the surface of a tube, (b) a carbon nanotube in a N doped area.

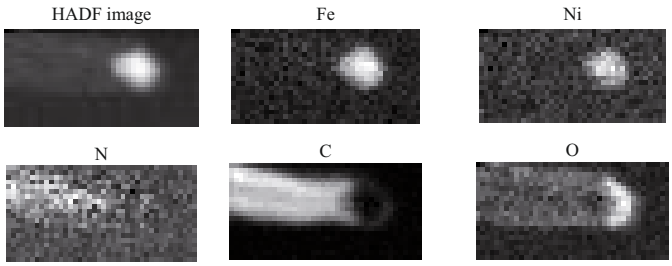

Fig. 4. HADF image and core-EELS elemental maps showing distribution of Fe, Ni, C, N and O in two-hour growth sample, as marked in Figure 1c. Spectra are taken in a grid of 64×64 pixels. Cr concentrations at the tube tip were below detection levels.

the surrounding carbon layers due to the complex intricate geometry). This indicates a quite rich CrN_x phase, as confirmed by the fine structure of the nitrogen core-loss signal, which consists of two strong peaks of roughly equal intensity at ∼399 and a doublet centred on 408 eV in the σ^* range (see Fig. 3). This is in good agreement with that reported in the literature for CrN [7]. Studies of chromium nitride films formed by ion beam-assisted deposition also suggest that CrN is the stable phase when excess nitrogen is present [8]. Cr undergoes rapid nitridation compared to carburisation, and the nitride phase is more stable than the carbide [9] (particularly under high [N] plasma conditions). This is consistent with our samples where the CrN signature never has any associated carbon signal.

The proximity of Fe and Cr particles suggests that both are initially present as a $FeCr_x$ alloy, but on absorbing nitrogen in the N rich environment of the plasma reactor the Cr nitrides forms CrN, which segregates from the FeCr alloy. We also observe pure Fe particles at nanotube tips, showing Fe-catalysed tube growth. This shows that the catalytic effect at 700 °C is optimum for Fe and not for Cr or a binary CrFe phase. Any carbon (including the tubes) is heavily decorated with both species of particles.

Ni was only detected in the two hour growth sample at very low concentrations, probably because significantly more Fe/Cr is sputtered, swamping any signal from nickel. In some cases this Ni dissolves in available Fe, for example it can be seen in low concentrations in the Fe particle in Figure 4. Oxygen contamination occurred primarily in the metal particles and disordered material, with some in the exterior of the nanotube walls. It appears that oxidation occurred after tube growth, since EELS shows that the oxygen is present in those metal particles decorating the outer tube walls but not in those at the tube core. Post-growth oxidation is also consistent with the oxidation of the exposed surface of the Fe particle at the nanotube tip shown in Figure 4.

4 Discussion

The limits of single walled nanotube growth by plasma techniques have been discussed recently [3]. Here we emphasize another constraint of plasma processing (this time for multi-walled nanotube growth), namely metal contamination of the deposit when driven by the grid biasing. Ion fluxes impinging on the substrate are controlled by biasing the grid [1,4] instead of the substrate-holder. This grid separates the ECR high density-low pressure plasma source from the deposition chamber. We recall that the plasma potential is always slightly higher than that of the grid. Therefore, when the grid is positively biased, the potential of the plasma directly follows the grid bias with respect to the grounded wall. Fixing the grid potential at +200 V, the plasma potential is ∼210 V, high enough to accelerate a large amount of ECR plasma ions to the chamber wall, especially in the magnetic trap area (the top of the reactor, details are given in Ref. [1]). Thus they induce the sputtering of the stainless steel wall and FeCr alloys are ejected from the top of the chamber down to the substrate. The grid transparency is about 50%, so less than half of this metallic vapour reaches the substrate, however, this is enough to catalyse nanotube growth.

On the basis of HADF and EELS observations it is possible to propose a growth model. Initially the major metal species are Fe and Cr atoms and $FeCr_x$ alloy particles. These particles are formed on the substrate, when metallic atoms and small sputtered metallic clusters deposit. The large amount of ammonia in the gas phase ensures many nitrogen radicals (NH_y, with $0 < y < 2$) which induce nitridation of $FeCr_x$, leading to the precipitation of CrN. In the well-studied process of nitridation of bulk stainless steels [9], such precipitation leads to internal stress in the material [10]. For nanoscale particles this stress can be relieved through segregation of the Fe and CrN. Meanwhile carbon from the surrounding gas feedstock dissolves in the Fe, eventually leading to conventional nanotube growth, separating the Fe and CrN phases. In cases where trace Ni was present from our initial experimental setup, this has the possibility to alloy with Fe and then co-catalyse nanotube growth.

The mechanism whereby the nanotube regions neighbouring the Cr particles can become highly nitrogen doped

is not clear. Depending on the efficiency of the ECR plasma, the nitrogen arriving at the sample consists of typically majority NH_3, ∼25% NH_x ($x < 3$) and a few at% N. Thus it could be that Cr is a particularly efficient catalyst at H removal, releasing nitrogen for bonding into the surrounding nanotube wall via the nearby Fe catalyst particle. Such nitrogen excess could be mobile in solid solution $Fe(N)_\alpha$ [11], providing a nitrogen source for the carbon nanotube. As the nanotube growth separates the Fe particle from the CrN, this surface diffusion route for N is cut and the nitrogen content in the tube drops. A less likely possibility is that the Cr is supersaturated with nitrogen, so as it cools the nitrogen is expelled into the surrounding environment, notably into neighbouring carbon structures; however if the tubes are already formed it is not clear how the N penetrates into the tube walls during cooling with this model.

5 Conclusions

We have studied nanotube samples produced via ECR plasma-assisted growth, using electron energy loss spectroscopy. Plasma sputtering of the stainless steel reaction chamber wall is revealed as undesired phenomenon present in grid driven PECVD processes, which can be inhibited by covering the chamber wall with graphite. When present, it introduces Cr and Fe into the reaction mixture, leading to unexpected rich reaction chemistry, particularly in grid driven systems when the grid bias exceeds 100 V. Nitridation of FeCr nanoparticles leads to segregation of CrN, while the Fe catalyses further nanotube growth. This is reminiscent of nitridation of bulk stainless steel surfaces.

The work highlights the importance of including chemical elemental analysis during growth studies in order to eliminate any possibility of misinterpretation of environmental contamination. In this respect, EELS is the ideal tool, providing both spatial and energetic resolution.

Although Cr is not directly involved in nanotube growth, our results suggest it may serve a useful role as a catalytic storage and release medium for nitrogen, leading to local high doping concentrations. In addition small supersaturated CrN_x particles may serve as a source of atomic N, absorbing NH_x from the gas phase, and following dehydrogenation, releasing atomic N for incorporation into the nanotubes. Low levels of Cr doping may be a way to produce heterogeneous high concentration nitrogen doped tubes. We note that Cr doping Ni is known to both increase its nitrogen solubility and diffusivity [12].

Thanks to Jean-Luc Duvail for useful discussions. CE acknowledges funding for part of this work from a Marie Curie Individual Research Fellowship of the European Community under contract number MCFI-2002-01436. This work was performed within the GDR-E “nanotubes” network.

References

1. T.M. Minea, S. Point, A. Gohier, A. Granier, Surf. Coat. Technol. **200**, 1101 (2005)
2. T.M. Minea, S. Point, A. Granier, M. Touzeau, Appl. Phys. Lett. **85**, 1244 (2004)
3. A. Gohier, T.M. Minea, A.M. Djouadi, A. Granier, M. Dubosc, Chem. Phys. Lett. **421**, 242 (2006)
4. T.M. Minea, S. Point, G. Popa, M. Touzeau, A. Granier, *Proc. 17 ESCAMPIG, Constanta, Romania, September 1–5 (2004),* 271
5. S. Point, T.M. Minea, B. Bouchet-Fabre, A. Granier, G. Turban, Diam. Relat. Mater. **14**, 891 (2005)
6. A. Gloter, A. Douiri, M. Tence, C. Colliex, Ultramicroscopy **96**, 385 (2003)
7. M. Sennour, Ph.D. thesis, INSA, Lyon (2002)
8. K. Volz, M. Kiuchi, W. Ensinger, Surf. Coat. Technol. **108-109,** 303 (1998)
9. H.J. Grabke, Mat. Corr. **56**, 384 (2005)
10. S.Y. Chang, U. Krupp, H.J. Christ, Mater. Sci. Eng. A **301**, 196-206 (2001)
11. S.S. Hosmani, R.E. Schacher, E.J. Mittemeijer, Mater. Sci. Tech.-Lond. **21**, 113 (2005)
12. H.-J. Christ, S.-Y. Chang, U. Krupp, Mat. Corr. **54**, 887 (2003)